DOE/BC/15202-1

(OSTI ID: 807240)

NMR Characterizations of Properties of Heterogeneous Media

A

Semi-Annual Progress Report

for the period

November 2001 - April 2002

Jinsoo Uh, Jack Phan, Song Xue, and A. Ted Watson

Department of Chemical Engineering, Texas A&M University

College Station, Texas 77843-3122

May 30, 2002

DOE Award Number DE-AC26-99BC15202

Texas Engineering Experiment Station (TEES)

Texas A&M University

College Station, Texas 77843-3122

Disclaimer

Abstract

The overall goal of this project is to develop reliable methods for resolving macroscopic properties important for describing the flow of one or more fluid phases in reservoirs from formation measurements. In Stage I, we develop advanced core analysis tools to determine macroscopic properties–the porosity, absolute, and relative permeability–within heterogeneous core samples. In Stage II we use these methods, together with additional NMR spectroscopic measurements, to obtain data for development of predictive methods. In Stage III, we develop improved relations for predicting permeabilities, and test a novel method for predicting relative permeability, from NMR well-log observable properties.

During this reporting period, the determination of surface relaxivity from NMR data is investigated. A new method for determining the surface relaxivity from measured data is developed and tested with data obtained from an Exxon sample. The new method avoids the use of a certain mathematical short-time approximation in the data analysis, which has been shown to be unsuitable.

Numerical work is in progress to simulate two-phase displacement experiments using all three spatial dimensions when estimating two-phase flow functions (relative permeability and capillary pressure properties). The modification of the computer code is underway with tests of the changes with specific examples.

Contents

List of Figures

1 Introduction

The detailed knowedge of rock and fluid properties is essential to the success of petroleum reservoir management and characterization. However, the study of heterogeneous media has been limited by the lack of methods to spatially resolve properties within porous media. Conventional methods utilize inflow and outflow measurements, and often do not adequately resolve heterogeneities. Nuclear magnetic resonance (NMR) spectroscopy and imaging (MRI) can give noninvasive measurements within media. Suitable interpretation of the data provides unprecedented opportunities for resolving fluid states to determine macroscopic properties important for describing the flow of one or more fluid phases in reservoirs.

In this project, we develop advanced core analysis tools utilizing MRI to determine macroscopic properties important for describing the flow of one or more fluid phases in reservoirs. We have been conducting a series of experiments on a suite of samples from a domestic reservoir, using the developed advanced core analysis tools to determine the basic properties. In addition, we are working on collecting other NMR experimental data from relaxation and diffusion experiments. We will obtain reliable estimates of relative permeability and capillary pressure functions from displacement experiments by accounting for property heterogeneities. Those data will be used to develop improved methods for predicting permeability from NMR observable parameters, and to test a novel method for predicting relative permeability from NMR measurements.

In this reporting period, we have continued to develop and implement a plan to remodel space to situate the new NMR equipment and laboratory at Colorado State University. Unavoidable delays by Facilities have pushed the delivery date back to July 15. For operation and maintenance of the new imager, a new research scientist will be involved and the position is now under search. There have been several academic achievements on the project topics during the period. An invited paper titled "NMR Determination of Porous Media Property Distributions" was submitted for publication in *Annual Reports on NMR Spectroscopy, Volume 48.* A technical presentation on simultaneous estimation of absolute and relative permeabilities from two-phase flow data will be presented at the *4th International Conference on Inverse Problems in Engineering* held in Angra dos Reis, Brazil, in May 2002.

We made advances in numerical and theoretical research, which are described in this report. In section 2, we present a new method to determine surface relaxivity. Our work on extending the current simulator to three-dimensional applications is described in section 3.

2 Determination of Surface Relaxivity

2.1 Introduction

The relaxation distribution is the basic NMR quantity used to characterize microscopic porous structures. Our research has been focused on determining pore-size distributions within porous media using characteristic relaxation times (Chang *et al.* 2000; Liaw *et al.* 1996). We have conducted a series of inversion recovery experiments on core samples and analyzed the data to determine T_1 relaxation distributions. The current issue is how to relate those distributions to pore-size distributions of the porous media.

In the fast-exchange limit (Brownstein and Tarr 1977), the pore-size (or surface-to-volume ratio, S/V) distribution and the T_1 distribution from an inversion recovery experiment can be directly related by the surface relaxivity, ρ:

$$\frac{1}{T_1} \;=\; \rho\,\frac{S}{V}. \tag{1}$$

Here, the effect of relaxation in the bulk phase is neglected because it is normally much slower than the relaxation at the solid-fluid surface. The surface relaxivity represents the strength of the surface/fluid interaction. Since NMR relaxation of fluid spins at solid surfaces is enhanced by a number of mechanisms that are system specific, the surface relaxivity should be determined to each system being examined. Relaxivities are normally experimentally determined by comparing NMR relaxation measurements to pore-size measurements made by techniques such as mercury injection and thin-section analysis (Brown *et al.* 1982; Gallegos *et al.* 1988). However, this is problematic since the reliability of such measures of pore-size is questionable.

In our approach, the PFGSE (Pulsed Field Gradient Spin Echo) technique is used to obtain the surface-to-volume ratio. The PFGSE NMR method has the advantages over other techniques that it is noninvasive and can sample the entire surface. A conventional PFG sequence consists of two identical gradient pulses of amplitude G, pulse width δ, and separation Δ, that are applied during two dephasing and rephasing periods of the spin-echo sequence (Stejskal and Tanner 1965). Under the narrow-pulse condition, $\delta \ll \Delta$, the pulse width is assumed short enough so that negligible molecular motion occurs during this period compared to that during Δ. Then, the time Δ between the gradient pulses is the time that the diffusional motion of molecules is traced. What we actually meaure from the PFGSE experiment is the magnitude of magnetization of the stimulated echo, M. The magnitude of stimulated echo depends on the diffusion time Δ and wave vector $\mathbf{k} = \delta\gamma\mathbf{g}$, where γ is gyromagnetic ratio and $\mathbf{g}$ is applied pulsed field gradient. The normalized magnitude of

magnetization with respect to the case $\mathbf{k} = \mathbf{0}$ is used to define time-dependent diffusivity, $D(\Delta)$:

$$D(\Delta) = -\frac{1}{\Delta} \lim_{k \to 0} \frac{\partial \log[M(k,\Delta)/M(0,\Delta)]}{\partial(k^2)}. \tag{2}$$

In Eq. (2) and what follows, the wave vector k is often written as a scalar with the understanding that the pulsed-field gradient is applied only along the axial direction. Mitra and Sen (1992) and Mitra *et al.* (1993) have shown that useful pore structure information can be obtained by studying time-dependent diffusivity at short diffusion time, which leads to

$$\frac{D(\Delta)}{D_0} \simeq 1 - \frac{4}{9\sqrt{\pi}} \frac{S}{V} \sqrt{D_0 \Delta}. \tag{3}$$

Here, S/V is surface-to-volume ratio within the porous media and D_0 is bulk diffusivity of the fluid. Equation (3) implies that the surface-to-volume ratio can be estimated by a set of time-dependent diffusivity data obtained at different short diffusion times. The time-dependent diffusivity is determined from experimental echo attenuation data using Eq. (2). In our previous work, we have estimated surface relaxivity by the average surface-to-volume ratio obtained from the stated analysis, $(S/V)^{av}$, and the average relaxation time, T_1^{av}:

$$\rho \;=\; \frac{1}{T_1^{av}\ (S/V)^{av}}. \tag{4}$$

We have reported some results of experimental analysis with our approach (Hollenshead *et al.* 2001; Liaw *et al.* 1996). While the method seems to work well with glass beads and some rock samples, the expected linear dependency of time-dependent diffusivity on the square root of diffusion time was not observed for Exxon samples. It was hypothesized that all the assumptions made in the analysis were not being met. The analysis assumes that the diffusion time is very short so that only the fraction $\sqrt{D_0\Delta}\ (S/V)^{av}$ of molecules "sense" the boundary. In practical experiments, however, it is not easy to obtain the stimulated echo data at very short times since the diffusion time is supposed to be larger than the RF (radio frequency) and gradient pulse widths. In addition, the diffusion time must be quite small in order to satisfy the short-time approximation when the pore-size is small and diffusion rate is fast. Therefore, we need to develop another methodology to predict surface relaxivity with data obtained at any diffusion times where the short-time approximation may not be valid.

In this reporting period, we developed a new method to estimate surface relaxivity using PFGSE experiments. A model of the PFGSE experiment which does not utilize a short-time approximation is used, and the surface relaxivity is found by solving an inverse problem. The method is advan-

tageous because all the stimulated echo data are used instead of using only those at small Δ, and the distribution of pore-sizes can be included in the model.

As will be shown in the following sections, pore-size distribution plays an important role in describing the PFGSE data obtained at diffusion times greater than those for which the short-time approximation is valid. In other words, we cannot properly describe those data with average surface-to-volume ratio or a single value of pore-size. Since the Exxon samples exhibit a broad distribution of pore-sizes, it is necessary to consider the effect of the distribution.

2.2 Modeling of PFGSE experiment

The amplitude of magnetization of a stimulated echo from PFGSE experiment is written as (Mitra and Sen 1992)

$$M(\mathbf{k},\Delta) = \frac{1}{V}\int G(\mathbf{r},\mathbf{r}',\Delta)e^{-i\mathbf{k}\cdot(\mathbf{r}-\mathbf{r}')}d\mathbf{r}d\mathbf{r}'. \tag{5}$$

Here, the RF and gradient pulses are assumed to be much narrower than the diffusion time Δ. The propagator $G(\mathbf{r},\mathbf{r}',t)$ is defined as the probability that a nuclei, which was initially at $\mathbf{r}'$, is to be found at $\mathbf{r}$ after time t. In order to find the explicit expression of $M(\mathbf{k},\Delta)$, we need some assumptions about the geometry of pores in the porous media. In our work, we make use of the isolated spherical pore model. Within the diffusion time region of our PFGSE experiment, it is reasonable to assume that the pores are isolated. The observation that pores in common rock samples are poorly coupled (Latour *et al.* 1992; McCall *et al.* 1991) supports this assumption. Spherical pore shape is profitable in that it is close to the actual pore shape and several studies on spherical pores are available (Mendelson 1986; Mitra and Sen 1992; Mitra *et al.* 1993; Cohen and Mendelson 1982; Valiullin and Skirda 2001).

Stimulated Echo from a Single Spherical Pore

The magnitude of magnetization of stimulated echo from PFGSE experiment on a single spherical pore of radius a can be derived as (Mitra and Sen 1992)

$$M(a;k,\Delta) = \sum_{n=0}^{\infty}\sum_{l=0}^{\infty}\frac{6(2l+1)\zeta_{ln}^2\exp(-D_0\Delta\zeta_{ln}^2/a^2)}{(\zeta_{ln}^2-k^2a^2)^2}\frac{(kaj_l'(ka)+\frac{\rho a}{D_0}j_l(ka))^2}{\left(\frac{\rho a}{D_0}-\frac{1}{2}\right)^2+\zeta_{ln}^2-\left(l+\frac{1}{2}\right)^2}. \tag{6}$$

Here, j_l is a spherical Bessel function of order l and the eigenvalue ζ_{ln} is the nth root of the following equation:

$$\zeta_{ln}j_l'(\zeta_{ln}) = -\frac{\rho a}{D_0}j_l(\zeta_{ln}). \tag{7}$$

Stimulated Echo from Spherical Pores with a Size Distribution

If a porous medium is composed of isolated spherical pores which have a size distribution, the fraction of fluid associated with pore-radii within $\log(a)$ and $\log(a) + d\log(a)$ is represented by $\mathcal{P}[\log(a)]d\log(a)$ (Lowell and Shields 1984; Liaw *et al.* 1996), where the pore-size distribution $\mathcal{P}$ satisfies

$$\int_{a=0}^{a=\infty} \mathcal{P}[\log(a)]\ d\log(a) = 1. \tag{8}$$

The total amount of magnetization from the whole sample is the summation of signals from all fluid in pores. Since fluid in each pore with radius a produce signal of $M(a;k,\Delta)$, the magnitude of the magnetization $M(k,\Delta)$ is calculated by

$$M(k,\Delta) = \int_{a=0}^{a=\infty} \mathcal{P}[\log(a)]\ M(a;k,\Delta)\ d\log(a). \tag{9}$$

The pore-size distribution $\mathcal{P}[\log(a)]$ is obtained from the T_1 distribution which is determined by an inversion recovery experiment. Considering $S/V = 3/a$ for a spherical pore of radius a and using Eq. (1), the T_1 distribution is related to pore-size distribution by

$$a = 3\rho T_1. \tag{10}$$

Since the surface area of spherical pores corresponding to the fluid volume fraction of $\mathcal{P}[\log(a)]\ d\log(a)$ is

$$\frac{4\pi a^2}{\frac{4}{3}\pi a^3}\mathcal{P}[\log(a)]\ d\log(a), \tag{11}$$

the average surface-to-volume ratio is obtained by

$$\left(\frac{S}{V}\right)^{av} = \int_{a=0}^{a=\infty} \frac{3}{a}\ \mathcal{P}[\log(a)]\ d\log(a). \tag{12}$$

If we define the average pore-radius of the porous system as

$$a^{av} = \frac{3}{(S/V)^{av}}, \tag{13}$$

a^{av} represents harmonic average of pore-radii with respect to $\log(a)$ distribution and Eq. (10) requires the average T_1, ${T_1}^{av}$, also to be a harmonic average so that

$$a^{av} = 3\rho T_1^{av} \tag{14}$$

is satisfied.

2.3 Estimation of Surface Relaxivity

In PFGSE experiments, we measure the relative magnitude of $M(k, \Delta)$. Thus, it is convenient to use the normalized magnetization with respect to the case $k = 0$:

$$Y = \frac{M(k, \Delta)}{M(0, \Delta)} \tag{15}$$

Combining equations (9) and (15), the normalized magnetization is calculated by

$$Y^{calc} = \frac{M(k, \Delta)}{M(0, \Delta)} = \frac{\int_{a=0}^{a=\infty} \mathcal{P}[\log(a)]\ M(a; k, \Delta)\ d\log(a)}{\int_{a=0}^{a=\infty} \mathcal{P}[\log(a)]\ M(a; 0, \Delta)\ d\log(a)} \tag{16}$$

if the surface relaxivity ρ is provided.

Equation (16) enables us to find the surface relaxivity by solving an inverse problem associated with the experimental data of the normalized magnetization, Y^{data}, and the calculated value, Y^{calc}. In this work, we estimate the surface relaxivity by minimizing the performance index J:

$$\min_{\rho} J = \| Y^{data} - Y^{calc} \|^2 . \tag{17}$$

2.4 Results and Discussion

Experimental Results

Inversion recovery experiments were performed on an Exxon sample (sample number 275) and the T_1 distribution is obtained by the methodology described in our previous report (Chang *et al.* 2000). Figure 1 shows the determined T_1 distribution of the sample. The area under an incremental part of the curve is directly proportional to the fraction of fluid associated with the corresponding characteristic time T_1 of longitudinal relaxation, and the whole area under the semi-log plot is unity. In Figure 1, the range of T_1 covers around two orders of magnitude. Equation (10) implies that the range of pore-sizes also has a broad distribution changing over two orders of magnitude. The harmonic average of T_1 of the distribution is calculated by

$$T_1^{av} = \left[\int_{T_1=0}^{T_1=\infty} \frac{1}{T_1} \mathcal{P}[\log(T_1)]\ d\log(T_1) \right]^{-1} = 0.074\ \text{sec}\,. \tag{18}$$

For the PFGSE experiment, we made use of a pulse sequence based on the "13-interval, Condition I" sequence of Cotts *et al.* (1989) (Fig. 2) to eliminate unwanted spin echoes by phase cycling. The diffusion time Δ is denoted by $\Delta = t_2 + 2\tau$ in the figure. For a half-sine gradient pulse of amplitude G and width δ, $k = \frac{4}{\pi}\gamma\delta G$. In our diffusion experiment, a series of $M(k, \Delta)$ are acquired by varing the amplitude of the gradient field while keeping the diffusion time constant. The same

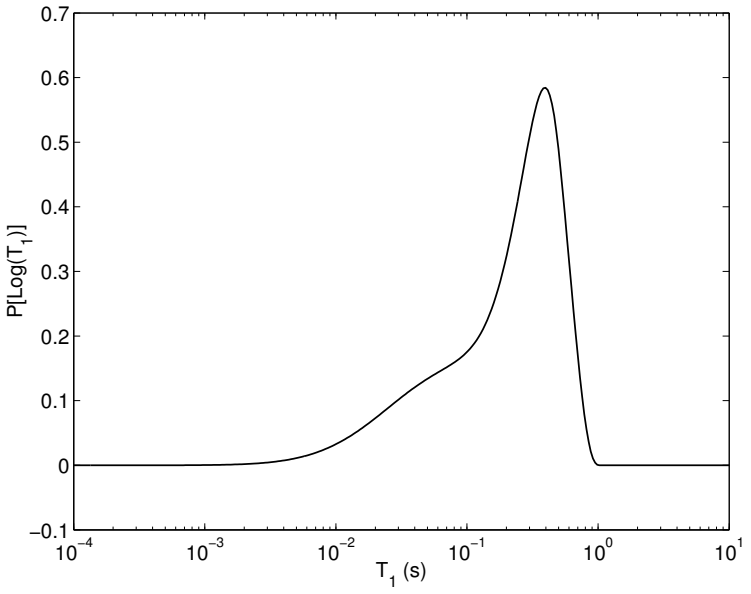

Figure 1: T_1 distribution of an Exxon sample (sample number 275)

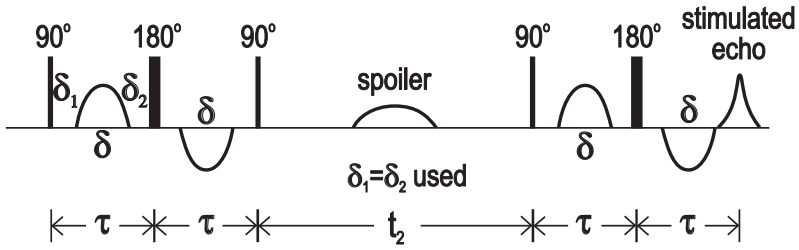

Figure 2: The "13-interval, Condition I" pulsed field gradient stimulated-echo pulse sequence.

procedure is repeated with four different diffusion times: $\Delta = 23$ ms, 38 ms, 58 ms, and 108 ms. The measured magnetization data of stimulated echoes are presented in Fig. 3. The logarithm of magnetization reduces as the gradient increases with different slopes depending on the diffusion time Δ. In our previous work, the initial slope at $k = 0$ associated with each diffusion time, Δ, has been used to obtain the time-dependent diffusivity $D(\Delta)$. The values of $D(\Delta)$ from the data in Fig. 3 are given in Table 1.

Estimation of Surface Relaxivity and Pore-Size Distribution

The surface relaxivity is estimated by the method described in section 2.3 using Eq. (17). Normalized magnetization is calculated with the optimum surface relaxivity and plotted in Fig. 3 with

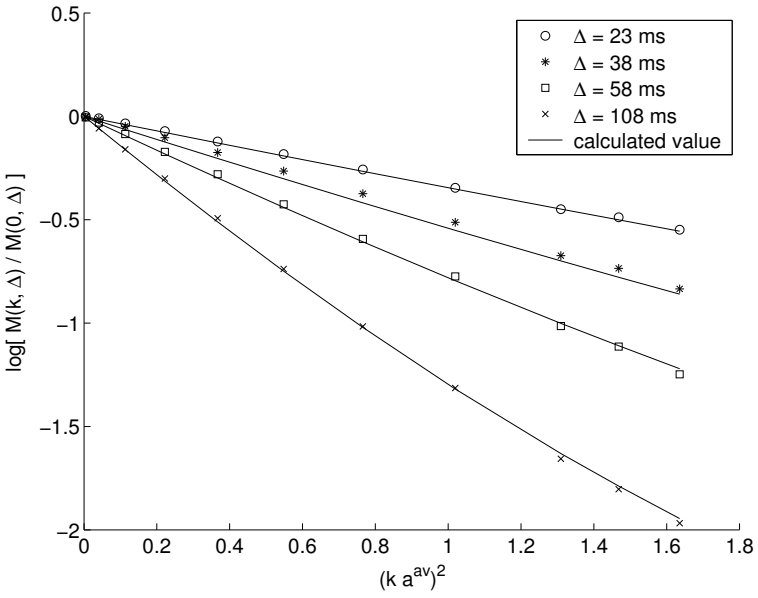

Figure 3: The logarithm of normalized magnetization data and the calculated values

Diffusion time Δ (ms)	Time-dependent diffusivity $D(\Delta)$ (10^{-5} cm^2/sec)	$D(\Delta)/D_0$ ($D_0 = 2.0\times10^{-5}$ cm^2/sec)
23	1.47	0.737
38	1.37	0.687
58	1.40	0.698
108	1.31	0.654

Table 1: Experimental time-dependent diffusivity

the experimental data. Table 2 summarizes the results of the surface relaxivity estimation. The pore-size distribution is obtained with the estimated surface relaxivity and presented in Fig. 4. The average pore-radius, a^{av}, in Fig. 3 and Table 2 is calculated as the harmonic average of radii of pores.

Discussion

The plot of the caculated values in Fig. 3 presents precise fit to the experimental data, which indicates that our assumptions used in the model are valid for describing the stimulated echo of the Exxon sample. The estimated pore-size distribution illustrated in Fig. 4 shows that the sample

Number of data used	44
Performance index, J	0.0145
Root mean square error	0.0181
Surface relaxivity, ρ	44 μm/sec
Average pore-radius, a^{av}	9.9 μm

Table 2: Results of surface relaxivity estimation

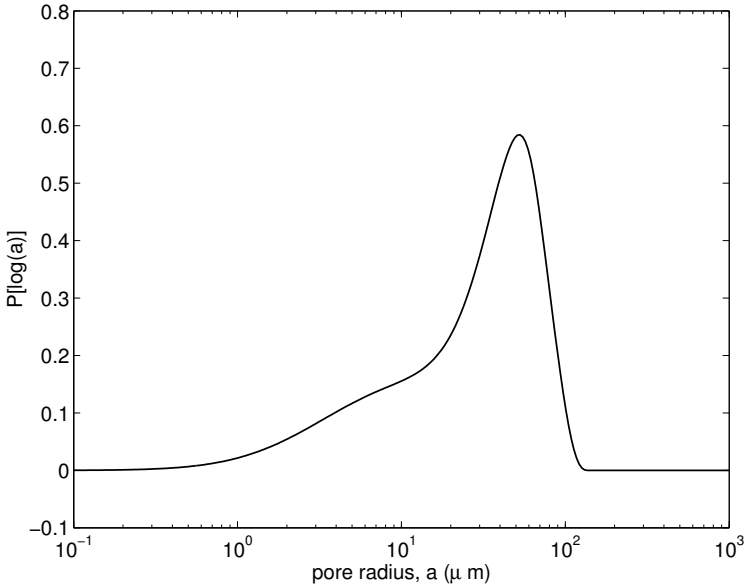

Figure 4: Pore-size distribution

has pores as small as a few microns.

It is instructive to validate the short-time approximation on this sample by calculating the time-dependent diffusivity from our simulation using Eq. (2). In order to observe the behavior of

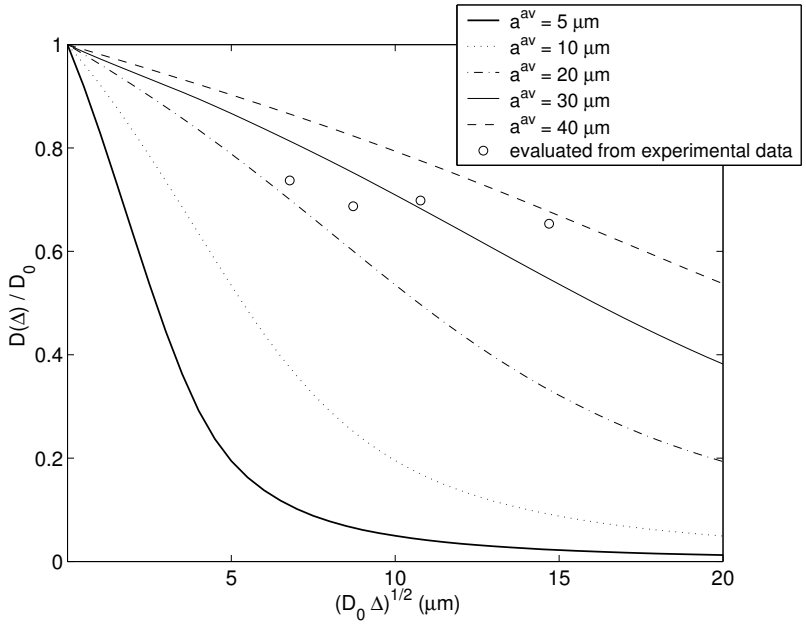

Figure 5: Simulated time-dependene diffusivity for a single pore of radius a^{av}

time-dependent diffusivity with respect to pore size, the time-dependent diffusivities for a single pore of different sizes are calculated and presented in Fig. 5. This case is equivalent to assuming that the pores have a uniform pore-size which is the average of the pore-size distribution. In conventional analysis of restricted diffusion, time-dependent diffusivity is often treated as a function of average surface-to-volume ratio and diffusion time. The superscript av of a in Fig. 5 is attached in this sense. Figure 5 shows that the time-dependent diffusivity has linear dependence on $\sqrt{D_0\Delta}$ at short diffusion time for all sizes of pores. As the diffusion time increases the time-dependent diffusivity tends to deviate from the linear behavior, and this deviation occurs earlier for smaller pores. Considering the Exxon sample has pores of a few microns, it is expected that all the pores in the sample cannot satisfy the linear dependency.

The non-linear behavior of time-dependent diffusivity can be explained using average pore-size as shown in Fig. 5. Thus we may be able to find the average surface-to-volume ratio and the corresponding surface relaxivity with data measured at any diffusion time. However, it can be shown that the time-dependent diffusivity expressed with average pore-size may not correctly

Number of data used	44
Performance index, J	0.127
Root mean square error	0.0537
Surface relaxivity, ρ	128 μm/sec
Average pore-radius, a^{av}	28.6 μm

Table 3: Results of surface relaxivity estimation using average pore size

predict the experimental diffusivity if the porous media has a broad distribution of pore-sizes. The experimentally evaluated time-dependent diffusivities of the Exxon sample (Table 1) are plotted in Fig 5. According to the figure, the experimental diffusivities do not match any of the calculated lines. The average pore size, a^{av}, corresponding to the experimental values would be about 30 μm. This average pore radius is much larger than the previously estimated value of $a^{av} = 9.9$ μm, where the pore-size distribution is used through an inverse problem. This result implies that we cannot estimate the correct surface relaxivity without considering the pore-size distribution for the Exxon sample.

The failure of the "average pore-size method" will be obvious when we estimate the surface relaxivity. Suppose a porous medium is composed of a uniform size of spherical pores. The calculated value of normalized magnetization is then given by

$$Y^{calc} = \frac{M(a^{av}; k, \Delta)}{M(a^{av}; 0, \Delta)}. \tag{19}$$

The average pore size is calculated by $a^{av} = 3\rho T_1^{av}$ (Eq. (14)) with a given surface relaxivity ρ. The same procedure previously described is applied to find the best value of surface relaxivity and the results are summarized in Table 3. We observe in Table 3 that the estimated surface relaxivity, $\rho = 128$ μm/sec, is considerably different from that in Table 2, $\rho = 44$ μm/sec. The calculated a^{av} is 28.6 μm, as is expected in Fig. 5. Comparing with Fig. 3, we find that the calculated values in Fig. 6 are not consistent with the measured data. Therefore, the assumption of single pore-size is not appropriate for describing the PFGSE data of the Exxon sample due to its broad distribution of pore-sizes.

The advantage of our new approach is effectively presented in Fig. 7. The dashed line represents the simulated time-dependent diffusivity values using pore-size distribution. Our simulation well describes the experimental time-dependent diffusivities which are evaluated from the PFGSE data.

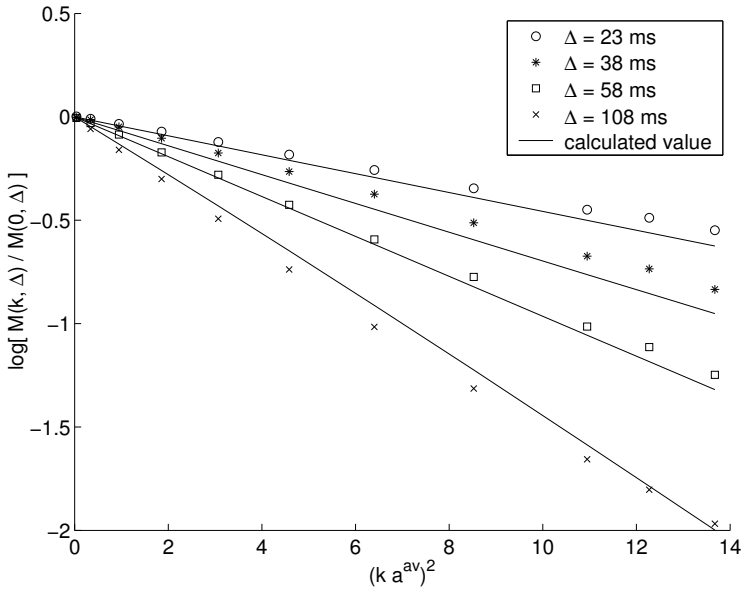

Figure 6: The logarithm of magnetization data and the calculated values using average pore size

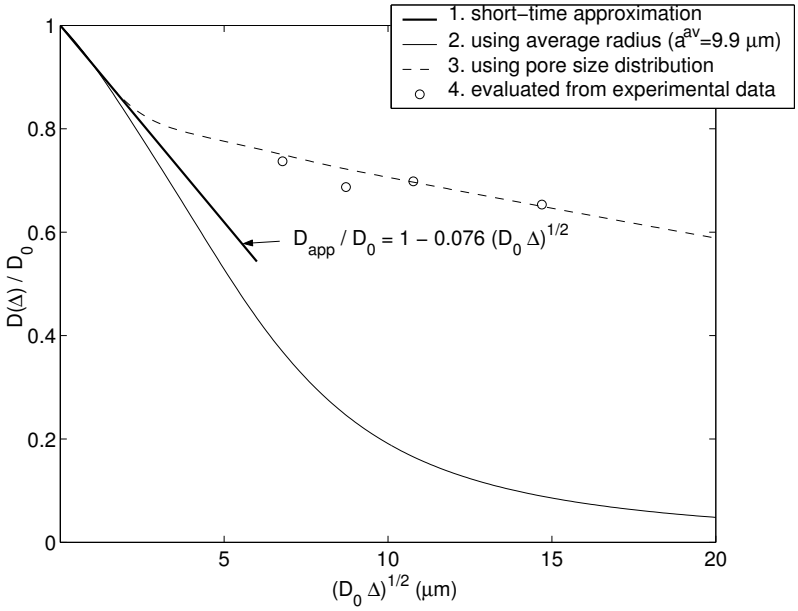

Figure 7: Comparisons of time-dependent diffusivities from different cases: 1. Short-time approximation, 2. Simulation assuming uniform pore-size and using average pore-radius, $a^{av} = 9.9\mu$m, 3. Simulation using pore-size distribution, 4. Evaluated values from experimental data

We could estimate the surface relaxivity by fitting the simulated diffusivities to the experimental values. However, this approach is problematic because the exact value of time-dependent diffusivity determined by Eq. (2) may depend on the strategy how we get the limiting value of magnetization at $k \to 0$ from the discrete data. In this work, we drew a smooth curve which best fit the data of each Δ and determined the initial slope. Those slope values will depend on the detailed form of the curve we choose. Our new approach is beneficial in that it utilizes all of the magnetization data with the same significance instead of only using the initial slope. At very short diffusion time, the dashed line shows linear dependency of time-dependent diffusivity on $\sqrt{D_0\Delta}$. The linear proportionality coincides with that of short-time approximation given in Eq. 3:

$$\begin{aligned} \frac{D(\Delta)}{D_0} &= 1 - \frac{4}{9\sqrt{\pi}} \left(\frac{S}{V}\right)^{av} \sqrt{D_0\Delta} \\ &= 1 - \frac{4}{9\sqrt{\pi}} \frac{3}{a^{av}} \sqrt{D_0\Delta} = 1 - 0.076\sqrt{D_0\Delta} \end{aligned} \tag{20}$$

This line of short-time approximation is drawn as a bold linear line in Fig. 7.

The thin linear curve in Fig. 7 is the simulated time-dependent diffusivity using a single pore-size value. If the Exxon sample studied had a uniform pore size which is equal to the average, $a^{av} = 9.9$ μm, the experimental time-dependent diffusivity would follow this curve. Due to the distribution of pore-sizes, the experimental time-dependent diffusivities are greater than the values predicted by average pore-size. If a porous medium has both larger and smaller pores, the molecules in larger pores diffuse longer distances than the average pore-size, although those in smaller pores have very restricted motion. This is the reason why the average pore-size model cannot properly explain the time-dependent diffusivity. Figure 7 illustrates that the simulated diffusivity curves coincide with the short-time approximation at very short time whether pore-sizes of the sample are uniform or have a broad distribution. Nevertheless, the diffusion time range of the coincidence is too short for short-time approximation to predict the experimental values of the Exxon sample.

3 Extension of Determination of Multiphase Flow Properties

3.1 Introduction

In this project, we intend to determine porosity and permeability distributions as a function of all three spatial coordinates, and to include that information in our procedure for determining the relative permeability and capillary pressure properties (multiphase flow functions). This will result

in more accurate estimates of those properties by suitably describing the effects of the heterogeneous properties when modeling the displacement experiments (Phan *et al.* 2001).

In order to fully represent the effects of heterogeneities, it is necessary that all three spatial dimensions are represented in the simulation of the experiment. Currently, only two-spatial dimensions are represented in SENDRA (Petec Software & Services 2000). We are modifying the code to include the third spatial dimension.

3.2 Theory

In the last report, we described the equations that involves our numerical work in three-dimensional problem. In this report, we repeat the primary equations and briefly describe the calculational procedure.

1. The mathematical model of the two-phase fluid flow in porous media (Kulkarni *et al.* 1998) is:

$$\frac{\partial \left(\phi \rho_l S_l\right)}{\partial t} = -\nabla \cdot \left(\rho_l \mathbf{v}_l\right) + q_l \qquad l = w \text{ or } nw \tag{21}$$

$$\mathbf{v}_l = -\frac{K k_{rl}}{\mu_l} \left(\nabla P_l - \rho_l \mathbf{g}\right) \tag{22}$$

with

$$P_c = P_w - P_{nw} \tag{23}$$

$$S_w + S_{nw} = 1 \tag{24}$$

where w and nw indicate the wetting-phase and non-wetting phase, respectively. The symbols are defined in the list of symbols on page 21.

2. The initial conditions are:

$$S_w\left(\mathbf{x}\right) = 1$$

$$P_w\left(\mathbf{x}\right) = P_{out}$$

where P_{out} is the pressure maintained at the outlet end.

3. Boundary Conditions

(a) The boundary conditions at the inlet (Fig. 8), $x = 0$ are:

$$\begin{aligned} q_{w,in} = & \int_A v_x dA \\ & = -\int_A \left(\frac{K k_{rw}}{\mu_w} \frac{\partial p}{\partial x} \right) dA \\ & = -\int_0^b \int_0^c \left(\frac{K k_{rw}}{\mu_w} \frac{\partial p}{\partial x} \right) dy\, dz \end{aligned}$$

where $q_{w,in}$ is the injection rate of the wetting-fluid phase.

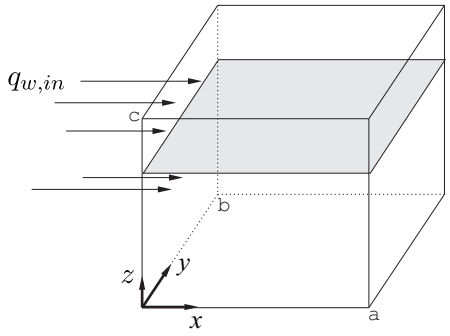

Figure 8: Boundary Conditions

(b) The boundary conditions at the outlet (Kulkarni *et al.* 1998), $x = a$, are:

$$\begin{aligned} \text{if} \quad P_c > 0 \quad & P_w = P_{out} \\ & \frac{\partial P_w}{\partial z} = 0 \\ \text{if} \quad P_c < 0 \quad & P_{nw} = P_{out} \\ & \frac{\partial P_{nw}}{\partial z} = 0 \\ \text{if} \quad P_c = 0 \quad & P_w = P_{nw} \\ & P_{nw} = P_{out} \end{aligned}$$

3.3 System matrix equations

The numerical method used to solve the mathematical model for two-phase flow is a finite difference, fully implicit method. The domain has $(N_x \times N_y \times N_z)$ grid blocks, where each block is represented by (i, j, k), $i = 1, 2, ..., N_x$, $j = 1, 2, ..., N_y$, and $k = 1, 2, ..., N_z$. For block (i, j, k), we obtain,

$$\left.\frac{\partial}{\partial x}\left(T\frac{\partial \Phi}{\partial x}\right)\right|_{i,j,k} = \frac{T_{i+\frac{1}{2},j,k}\left(\Phi_{i+1,j,k}-\Phi_{i,j,k}\right)-T_{i-\frac{1}{2},j,k}\left(\Phi_{i,j,k}-\Phi_{i-1,j,k}\right)}{(\Delta x)^2}$$
$$= \frac{1}{(\Delta x)^2}\left\{\Phi_{i-1,j,k}\left(T_{i-\frac{1}{2},j,k}\right)+\Phi_{i,j,k}\left(-T_{i-\frac{1}{2},j,k}-T_{i+\frac{1}{2},j,k}\right)+\Phi_{i+1,j,k}\left(T_{i+\frac{1}{2},j,k}\right)\right\}$$

$$\left.\frac{\partial}{\partial y}\left(T\frac{\partial \Phi}{\partial y}\right)\right|_{i,j,k} = \frac{1}{(\Delta y)^2}\left\{\Phi_{i,j-1,k}\left(T_{i,j-\frac{1}{2},k}\right)+\Phi_{i,j,k}\left(-T_{i,j-\frac{1}{2},k}-T_{i,j+\frac{1}{2},k}\right)+\Phi_{i,j+1,k}\left(T_{i,j+\frac{1}{2},k}\right)\right\}$$

$$\left.\frac{\partial}{\partial z}\left(T\frac{\partial \Phi}{\partial z}\right)\right|_{i,j,k} = \frac{1}{(\Delta z)^2}\left\{\Phi_{i,j,k-1}\left(T_{i,j,k-\frac{1}{2}}\right)+\Phi_{i,j,k}\left(-T_{i,j,k-\frac{1}{2}}-T_{i,j,k+\frac{1}{2}}\right)+\Phi_{i,j,k+1}\left(T_{i,j,k+\frac{1}{2}}\right)\right\}$$

After performing the discretization for the equations (21)–(24), we establish the system equations to solve our problem (Faust and Mercer 1997):

$$\{F(\mathbf{X}_{i,j,k})\}^{n+1} = \{f(\mathbf{X}_{i,j,k})\}^{n+1} - \{h(\mathbf{X}_{i,j,k})\}^{n+1} + \{h(\mathbf{X}_{i,j,k})\}^{n} + Q_{i,j,k}^{n+1} = 0 \tag{25}$$

in which:

$$f(\mathbf{X}_{i,j,k}) = \left\{\ \Delta_x\left(T\Delta_x\Phi\right)+\Delta_y\left(T\Delta_y\Phi\right)+\Delta_z\left(T\Delta_z\Phi\right)\ \right\}_{i,j,k}$$
$$(\mathbf{X}_{i,j,k}) = \frac{1}{\Delta_t}\left(\phi bS\right)_{i,j,k}$$

where $\mathbf{X}_{i,j,k} \equiv (P_o, S_w)_{i,j,k}$ is a solution at the block (i,j,k), P_o and S_o are oil pressure and water saturation, respectively.

The system equation (25) is a non-linear system of equations. In order to linearize this system equation we use the Taylor series to expand the functions, $f(\mathbf{X})$ and $h(\mathbf{X})$ (Eq. 25). In the expansion of $f(\mathbf{X})$ and $h(\mathbf{X})$, we take the partial derivative with respect to the vector, (P_o, S_w) . After performing the linearization, we obtained the linear system equations:

$$\mathbf{J}^n\delta\mathbf{X}^{n+1} = -F(\mathbf{X})^n - \mathbf{W}^n$$
$$\mathbf{X}^{n+1} = \mathbf{X}^n + \delta\mathbf{X}^{n+1}$$

where $\mathbf{W}$ is a matrix which is determined by initial and boundary conditions.

The matrix $\mathbf{J}$ in the above equation is the Jacobian matrix of the system function $F_{i,j,k}(\mathbf{X}) \equiv F(\mathbf{X}_{i,j,k})$ at each block (i,j,k). The matrix $\mathbf{J}$ is a square matrix with dimension $(N \times N)$, $N = N_x \times N_y \times N_z$, and each term of matrix $\mathbf{J}$ is also a 2×2 matrix.

3.4 Calculational procedure

We here briefly describe the calculational procedure to solve the forward problem.

1. Derive the governing equation,

$$\frac{\partial \left(\phi \rho_l S_l\right)}{\partial t} = -\nabla \cdot \left(\rho_l \mathbf{v}_l\right) + q_l$$

2. Derive the discrete equations (Peaceman 1977),

$$\left\{\Delta_x \left(T \Delta_x \Phi\right) + \Delta_y \left(T \Delta_y \Phi\right) + \Delta_z \left(T \Delta_z \Phi\right)\right\}^{n+1} = \frac{1}{\Delta_t}\left\{\left(\phi b S\right)^{n+1}\right\} - \frac{1}{\Delta_t}\left\{\left(\phi b S\right)^{n}\right\} - Q$$

3. Establish and obtain the system equations,

$$\left\{F(\mathbf{X})\right\}^{n+1} = \left\{f(\mathbf{X})\right\}^{n+1} - \left\{h(\mathbf{X})\right\}^{n+1} + \left\{h(\mathbf{X})\right\}^{n} + \mathbf{Q}^{n+1} = 0$$

4. Use the B-splines to represent the property functions (Schumaker 1981; Bartels *et al.* 1987)

5. From the boundary conditions and initial guess, the solution $\mathbf{X}^{n+1} \equiv (\mathbf{P}_o, \mathbf{S}_w)$ is to be found in the following equation,

$$\mathbf{J}^n \delta \mathbf{X}^{n+1} = -F(\mathbf{X})^n - \mathbf{W}^n$$

$$\mathbf{X}^{n+1} = \mathbf{X}^n + \delta \mathbf{X}^{n+1}$$

3.5 Matrix Structures and Matrix Solvers

The Jacobian matrix, $\mathbf{J}$, is established from the fully implicit finite-difference method. This matrix is a block sparse matrix, and its terms are 2×2 matrices. The matrix $\mathbf{J}$'s structure for one, two, and three-dimensional representations is shown in Fig. (9).

Currently, only two-spatial dimensional problems are represented in SENDRA (Petec Software & Services 2000). For one-dimensional problems, the Thomas algorithm is used to solve the block system equations. For two-dimensional problems, a sparse matrix technique (Aziz and Settari 1979) is used to solve the equations. In addition, the technique of D4 ordering (Aziz and Settari 1979) is applied in two-dimensional problems. This D4 technique provides the greatest advantage (Aziz and Settari 1979) for two-dimensional reservoir simulation, especially for complex reservoir shapes. But our problem is one of three-dimensional simulation for fluid flow through a laboratory sample which has a regular shape. Therefore, the D4 ordering technique does not provide an advantage for our problem.

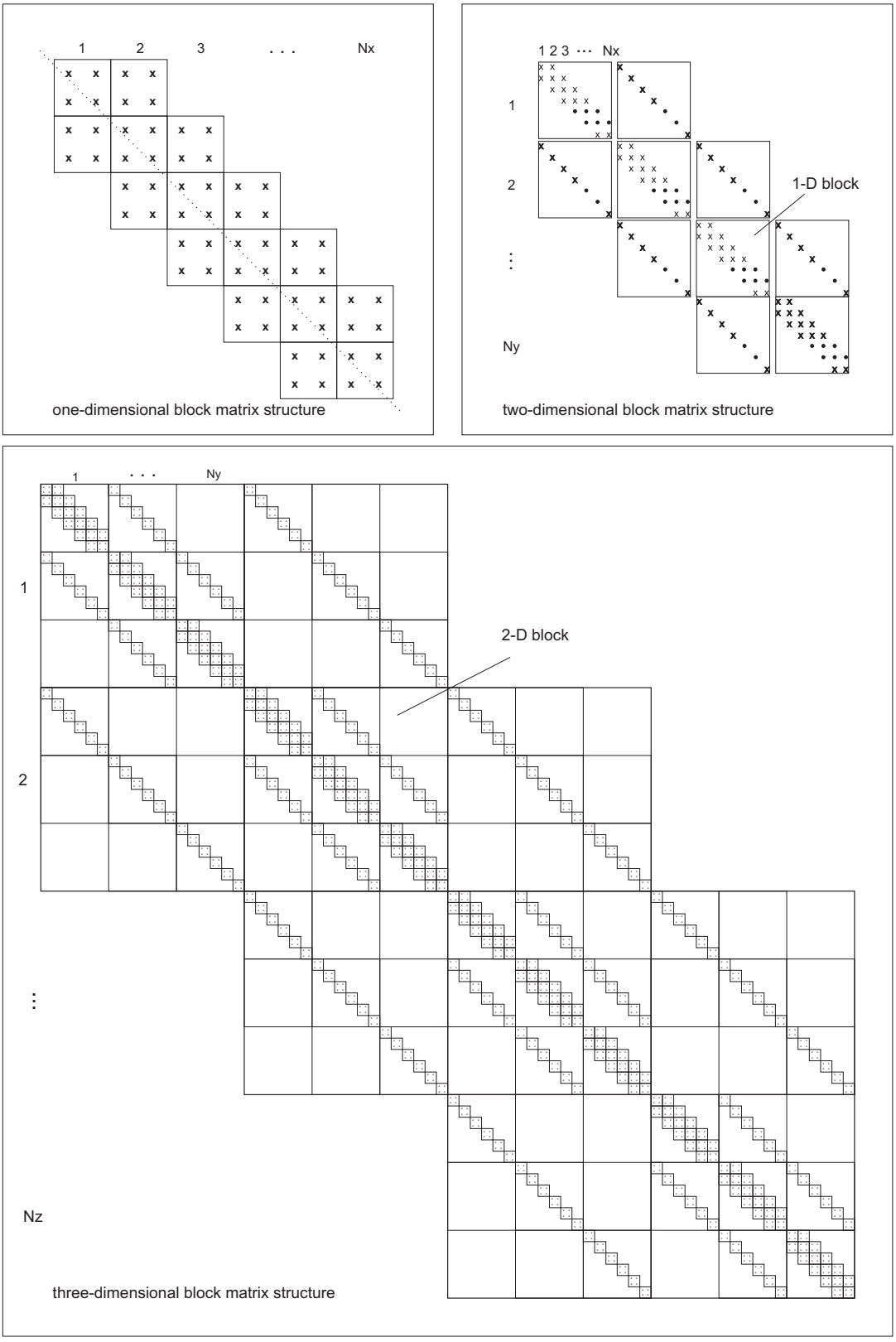

Figure 9: Jacobian block matrix structure

In order to handle our three-dimensional simulation in SENDRA, we applied the sparse matrix technique of the matrix solver, SPLIB (linear of sparse iterative solver) (Bramley and Wang 1995). In addition, we have used the sparse matrix library (Saad 1994), SPARSKIT (a basis tool kit for sparse matrix computations), to write the code for changing the original IJ value format (matrix output format from SENDRA, which is defined in Sparse Matrix Manipulation System (Alvarado 1993)) into Harwell-Boeing format (Duff *et al.* 1992) before using the library SPLIB. Figure (10) shows the working flowchart for our three-dimensional simulation.

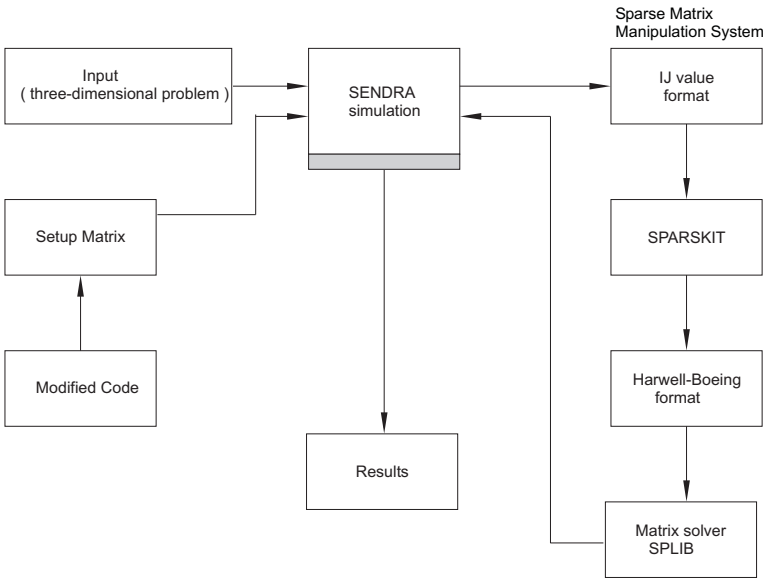

Figure 10: Working flowchart for three-dimensional simulation

3.6 Results and Discussion

In the current reporting period, our group is in progress of the numerical work to extend the numerical simulator used to determine relative permeability and capillary pressure functions to three dimensions. After replacing the matrix solver in SENDRA with SPLIB (see Fig. 10), we have performed tests for one and two-dimensional problems. As desired, our results are the same as those obtained with the original version of SENDRA. The next step is to make changes in SENDRA to perform simulation of three-dimensional problems. The modified code will be integrated with SENDRA to perform three-dimensional applications. We will finish the above numerical task and present the results in the final report.

4 Conclusions

The objectives of this research project are to develop various unique capabilities of NMR imaging and spectroscopic techniques for probing macroscopic properties important for describing the flow of one or more fluid phases in heterogeneous media. At the end of the current reporting period, several tasks have been accomplished or initiated.

We have conducted theoretical research on determining surface relaxivity using a NMR PFGSE method. We presented a new method for the estimation of surface relaxivity, where some assumptions previously made were removed. We introduced simulation of the PFGSE experiment and the surface relaxivity was found by solving an inverse problem. This method is not restricted by a short-time approximation. The new approach enables us to include the effect of a distribution of pore-sizes in the model, and as a result, it gives improved estimates of surface relaxivity and the corresponding pore-size distributions.

The computer code (SENDRA) currently used to simulate two-phase displacement experiments is limited to one or two spatial dimension problems. Numerical work is in progress to extend the simulator to three-dimensional applications. After replacing the matrix solver with SPLIB, SENDRA is able to solve the sparse matrix which is raised by three-dimensional problems. We have tested SENDRA with the SPLIB for one and two dimensional problems. As expected, the test results are same as those obtained with the original version of SENDRA. To simulate three-dimensional problems, the source code of SENDRA has been modified. The next step is to integrate the modified code with SENDRA and perform the three-dimensional cases. The current progress is satisfactory. We will finish the above numerical task and present the results in the final report.

List of Symbols

γ	gyromagnetic ratio
δ	width of RF pulse
Δ	diffusion of fluid
ρ	surface relaxivity in section 2
	fluid density in section 3
ϕ	porosity
a	pore radius
D	diffusivity
D_Δ	time-dependent diffusivity
$\mathbf{g}$	pulsed field gradient in section 2
	earth gravity acceleration in section 3
G	propagator
J	performance index
$\mathbf{k}$	wave vector
k_r	relative permeability
K	absolute permeability
M	magnitude of magnetization of stimulated spin echo
N_x	number of blocks in x direction
N_y	number of blocks in y direction
N_z	number of blocks in z direction
P	pressure
$\mathcal{P}$	pore-size or T_1 distribution
q	sink or source inside the domain
$\mathbf{r}$	position vector
S	surface area of pores in section 2
	saturation in section 3
T_1	characteristic time of longitudinal relaxation
V	volume of pores

Superscript :

av	average
n	time step index

Subscript :

c	capillary
i	spatial index in x direction
j	spatial index in y direction
k	spatial index in z direction
l	fluid index (water or oil)
o	oil
t	indicated time
w	water

Bold Symbol indicates a vector or matrix

References

Alvarado, F. L. (1993). The sparse matrix manipulation system, user and reference manual . URL address: http://www.cs.indiana.edu/ftp/techreports/tr454.html.

Aziz, K. and A. Settari (1979). *Petroleum Reservoir Simulation*. London: Applied Science Publishers.

Bartels, R. H., J. C. Beatty, and B. A. Barsky (1987). *An Introduction to Splines for use in Computer Graphics & Geometric Modeling*. Morgan Kaufmann.

Bramley, R. and X. Wang (1995). SPLIB: A library of iterative methods for sparse linear systems . URL address: http://www.elk.itu.edu.tr/ dag/lssmc.html.

Brown, J. A., L. F. Brown, J. A. Jackson, J. V. Milewski, and B. J. Travis (1982). NMR logging tool development: Laboratory studies of tight gas sands and artificial porous material. *SPE/DOE 10823*, 203.

Brownstein, K. R. and C. E. Tarr (1977). Spin-lattice relaxation in a system governed by diffusion. *J. Mag. Res. 26*, 17.

Chang, C. T., C. Choi, J. T. Hollenshead, and A. T. Watson (2000, June). NMR characterizations of properties of heterogeneous media. Research Report. U. S. Department of Energy, Report Number DE-AC26-99BC15202, Texas A&M University.

Cohen, M. H. and K. S. Mendelson (1982). Nuclear magnetic relaxation and the internal geometry of sedimentary rocks. *J. Appl. Phys. 52*, 1127.

Cotts, R. M., M. J. R. Hoch, T. Sun, and J. T. Markert (1989). Pulsed field gradient stimulated echo methods for improved NMR diffusion measurements in heterogeneous systems. *J. Mag. Res. 83*, 252.

Duff, I. S., R. G. Grimes, and J. G. Lewis (1992). Users's guide for the Harwell-Boeing sparse matrix collection.

Faust, C. R. and J. W. Mercer (1997). Finite-difference model of two-dimensional, single-, and two-phase heat transport in a porous medium- version 1. Research Report Open-File Report 77-234, U.S. Geological Survey.

Gallegos, D. P., D. M. Smith, and C. J. Brinker (1988). An NMR technique for the analysis of pore structure: Application to mesopores and micropores. *J. Coll. Interface Sci. 124*, 186.

Hollenshead, J. T., J. Phan, J. Uh, and A. T. Watson (2001, May). NMR characterizations of properties of heterogeneous media. Research Report. U. S. Department of Energy, Report Number DE-AC26-99BC15202, Texas A&M University.

Kulkarni, R. N., A. T. Watson, J. E. Nordtvedt, and A. Sylte (1998). Two-phase flow in porous media: Property identification and model validation. *AIChE J. 44*, 2337.

Latour, L. L., R. L. Kleinberg, and A. J. Sezginer (1992). Nuclear magnetic resonance properties of rocks at elevated temperatures. *J. Coll. Interface Sci. 150*, 535.

Liaw, H.-K., R. N. Kulkarni, S. Chen, and A. T. Watson (1996). Characterization of fluid distributions in porous media by NMR techniques. *AIChE J. 42*, 538.

Lowell, S. and J. E. Shields (1984). *Powder Surface Area and Porosity*. New York, NY: Chapman and Hall.

McCall, K. R., D. L. Johnson, and R. A. Guyer (1991). Magnetization evolution in connected pore systems. *Phys. Rev. B 44*, 7344.

Mendelson, K. S. (1986). Nuclear magnetic relaxation in porous media. *J. Electrochem. Soc. : Solid State and Technology 133*, 631.

Mitra, P. P. and P. N. Sen (1992). Effects of microgeometry and surface relaxation on NMR pulsed-field-gradient experiments: Simple pore geometries. *Phys. Rev. B 45*, 143.

Mitra, P. P., P. N. Sen, and L. M. Schwartz (1993). Short-time behavior of the diffusion coefficient as a geometrical probe of porous media. *Phys. Rev. B 47*(14), 8565.

Peaceman, D. W. (1977). *Fundamentals of Numerical Reservoir Simulation*. NewYork: Elsevier Scientific Publishing Company.

Petec Software & Services (2000). *CENDRA Verison 1.4 User's Manual*. Bergen, Norway.

Phan, J., J. Uh, R. Valestrand, S. Xue, and A. T. Watson (2001, November). NMR characterizations of properties of heterogeneous media. Research Report. U. S. Department of Energy, Report Number DE-AC26-99BC15202, Texas A&M University.

Saad, Y. (1994). SPARSKIT: a basis tool kit for sparse matrix computations, version 2 . URL address: http://www.cs.umn.edu/research/arpa/sparskit/sparskit.html.

Schumaker, L. L. (1981). *Spline Functions: Basic Theory*. John Wiley and Sons.

Stejskal, E. O. and J. E. Tanner (1965). Spin diffusion measurements: Spin echoes in the presence of a time-dependent field gradient. *J. of Chem. Phys. 42*, 288.

Valiullin, R. and V. Skirda (2001). The dependent self-diffusion coefficient of molecules in porous media. *J. of Chem. Phys. 114*, 452.